

# Optically Thin Core Accretion: How Planets Get Their Gas in Nearly Gas-Free Discs

Eve J. Lee<sup>1,2\*</sup>, Eugene Chiang<sup>1,3</sup>, Jason W. Ferguson<sup>4</sup>

<sup>1</sup>*Astronomy Department, University of California Berkeley, Berkeley, CA 94720-3411, USA*

<sup>2</sup>*TAPIR, Walter Burke Institute for Theoretical Physics, Mail Code 350-17, Caltech, Pasadena, CA 91125, USA*

<sup>3</sup>*Department of Earth and Planetary Science, University of California Berkeley, Berkeley, CA 94720-4767, USA*

<sup>4</sup>*Physics Department, Wichita State University, Wichita, KS 67260-0032, USA*

## ABSTRACT

Models of core accretion assume that in the radiative zones of accreting gas envelopes, radiation diffuses. But super-Earths/sub-Neptunes ( $1\text{--}4R_{\oplus}$ ,  $2\text{--}20M_{\oplus}$ ) point to formation conditions that are optically thin: their modest gas masses are accreted from short-lived and gas-poor nebulae reminiscent of the transparent cavities of transitional discs. Planetary atmospheres born in such environments can be optically thin to both incident starlight and internally generated thermal radiation. We construct time-dependent models of such atmospheres, showing that super-Earths/sub-Neptunes can accrete their  $\sim 1\%$ -by-mass gas envelopes, and super-puffs/sub-Saturns their  $\sim 20\%$ -by-mass envelopes, over a wide range of nebular depletion histories requiring no fine tuning. Although nascent atmospheres can exhibit stratospheric temperature inversions effected by atomic Fe and various oxides that absorb strongly at visible wavelengths, the rate of gas accretion remains controlled by the radiative-convective boundary (rcb) at much greater pressures. For dusty envelopes, the temperature at the rcb  $T_{\text{rcb}} \simeq 2500$  K is still set by  $\text{H}_2$  dissociation; for dust-depleted envelopes,  $T_{\text{rcb}}$  tracks the temperature of the visible or thermal photosphere, whichever is deeper, out to at least  $\sim 5$  AU. The rate of envelope growth remains largely unchanged between the old radiative diffusion models and the new optically thin models, reinforcing how robustly super-Earths form as part of the endgame chapter in disc evolution.

**Key words:** planets and satellites: formation

## 1 INTRODUCTION

The *Kepler* mission has revealed that about half of all Sun-like stars harbor at least one planet with an orbital period  $< 85$  days (Howard et al. 2010; Batalha et al. 2013; Petigura et al. 2013; Dong & Zhu 2013; Fressin et al. 2013; Rowe et al. 2014; Burke et al. 2015). The most common of these are the super-Earths, here defined as having radii between 1 and  $4 R_{\oplus}$ .<sup>1</sup> Transit-timing analyses (Wu & Lithwick 2013) and radial velocity surveys (Weiss & Marcy 2014) have determined that the masses of super-Earths range from  $\sim 2$  to

$20M_{\oplus}$ , with most having masses  $\lesssim 6M_{\oplus}$ . To be consistent with the observed masses and radii, the largest-size super-Earths must have gas envelopes overlaying their solid cores. Gas-to-core mass ratios (GCRs) are estimated to be between  $\sim 0.1\text{--}10\%$ , and are more typically  $\sim 1\%$  (Lopez & Fortney 2014; Wolfgang & Lopez 2015).

The GCRs of super-Earths are neither as low as those of solar system terrestrial planets, nor as high as those of gas giants. They imply a formation history intermediate in time between these populations: neither so late that the parent circumstellar disc has lost all its gas, nor so early that the disc is still gas-rich.<sup>2</sup> This scenario, however, would seem to introduce a fine-tuning problem. Why are GCRs on the order

\* Contact e-mail: [evelee@caltech.edu](mailto:evelee@caltech.edu)

<sup>1</sup> Planets with radii between  $\sim 2\text{--}4 R_{\oplus}$  are sometimes called “mini-Neptunes” to distinguish them from  $\sim 1\text{--}2 R_{\oplus}$  super-Earths. These two populations are indeed observed to be distinct (e.g., Fulton et al. 2017), a consequence of the former having retained their atmospheres and the latter have lost them (e.g., Owen & Wu 2013, 2017; Ginzburg et al. 2017; see also our section 4.2). Since we are interested in how these planets acquired their atmospheres in the first place (pre-mass loss), we will not make this distinction but lump all under the common banner of super-Earths.

<sup>2</sup> More specifically, we posit that cores form during the “giant impact” era when gas dynamical friction was sufficiently weak to permit protocores to cross orbits and merge; relevant nebular densities are lower than those of the standard solar-composition minimum-mass disc by four orders of magnitude and possibly more depending on the exact orbital spacing between protocores (see, e.g., Lee & Chiang 2016, their Figures 5 and 6).

of 1%? At what precise point in the parent nebula’s depletion history did super-Earths appear? How can we guarantee that at that point in history there was enough disc gas for super-Earth cores to acquire their percent-by-weight atmospheres?

This problem of having to fine-tune the nebular density is illusory. Recent studies of how planets get their gas (Lee et al. 2014; Lee & Chiang 2015, 2016; Ginzburg et al. 2016) have shown that the rate at which nebular gas accretes onto cores is remarkably insensitive to the nebular density. According to these models, the nebula can be depleted over a wide range of values—anywhere from one to nine orders of magnitude relative to a standard solar-composition “minimum-mass” disc—and super-Earths will still emerge with final GCRs of 1–10% (e.g., Figures 4–6 of Lee & Chiang 2016). Nor is there any particular fine-tuning problem in time: the duration of gas accretion can last anywhere from  $\sim 0.1$ –1 Myr, with even shorter durations allowed for GCR  $\sim 0.1\%$ . These gas accretion timescales fit nicely with the timescales over which discs finally clear; i.e., the duration of the “transitional” disc phase, which is about 10% of the total disc lifetime (Figure 9 of Owen et al. 2011; Alexander et al. 2014; see also Figure 11 of Espaillat et al. 2014).

The fundamental reason why percent-by-weight atmospheres abound is because cooling times of percent-by-weight atmospheres are of order gas disc dispersal times of  $\sim 0.1$ –1 Myr. Planetary atmospheres can only grow as much as they can cool. The envelope cooling (= accretion) history is insensitive to the exact value of the outer nebular density because the rate of cooling is not controlled near the Hill or Bondi sphere radius where the atmosphere connects to the nebula; the cooling is controlled instead much deeper in the planet’s envelope, at its radiative-convective boundary (rcb). The rcb is the “lid” that regulates how much energy is released from the planet. That energy is concentrated in the convective interior, which dominates the mass of the envelope. Below the rcb, convection can carry an arbitrarily large energy flux outward. But above the rcb, the outward flux from radiative diffusion can only be as large as the local temperature gradient allows. That gradient equals its maximum possible value—namely the adiabatic value—at the rcb (by definition; if it were larger, convection would ensue, and the rcb would be located at higher altitude). Thus the rcb acts to throttle the flux emerging from the convective interior.

The properties of the rcb—its temperature  $T_{\text{rcb}}$  and density  $\rho_{\text{rcb}}$ , and by extension its opacity—do not much depend on  $\rho_{\text{out}}$ , the density of the nebula at large. If the outermost portion of a planet’s envelope contains significant amounts of dust, the rcb materializes at the  $\text{H}_2$  dissociation front, and so  $T_{\text{rcb}} \simeq 2500$  K (Lee et al. 2014). In a dust-free envelope, the outer radiative layer is nearly isothermal with the nebula, and so  $T_{\text{rcb}}$  is set by the external nebular temperature  $T_{\text{out}}$ . In either case, whether the envelope is dusty or dust-free, the density  $\rho_{\text{rcb}}$  is controlled essentially by the adiabat in the convective zone below the rcb. Because energy is spent dissociating  $\text{H}_2$  in the convective zone rather than heating the gas, the adiabatic index  $\gamma_{\text{ad}}$  is driven closer to unity; in particular,  $\gamma_{\text{ad}} < 4/3$ , which renders the convective zone centrally concentrated, with the bulk of the envelope mass residing just above the surface of the underlying core (Lee & Chiang 2015). The consequence is that  $\rho_{\text{rcb}}$  is determined by the envelope mass, the core mass and radius,

the adiabatic index, and  $T_{\text{rcb}}$  (equation 11 of Lee & Chiang 2015). None of these factors depends on  $\rho_{\text{out}}$ .

The above analysis would be complete were it not for the fact that it relies on models that may occasionally be unphysical in the following sense. Every model of core accretion from the nebula of which we are aware (going back to, e.g., Pollack et al. 1996) utilizes the equation of radiative diffusion to describe energy transport in the radiative zone of the planetary envelope. The diffusion approximation is valid wherever the gas is optically thick (in a Rosseland mean sense) to the local thermal radiation field. Applicable settings include nascent Jupiters embedded in gas-rich nebulae. But super-Earths take us into a new parameter space: they are spawned from discs that are heavily (but not completely) depleted of gas and dust, reminiscent of the inner cavities of transitional discs. In particular, core formation by giant impacts demands nebular gas to be depleted by factors of  $\gtrsim 10^4$  to defeat gas dynamical friction (see, e.g., Lee & Chiang 2016, their Figures 5 and 6). Not only are such discs potentially optically thin (see Figure 1), but the planetary envelopes themselves may be as well, both to incoming starlight and outgoing thermal radiation.

Under optically thin conditions, the diffusion approximation must be replaced by more sophisticated treatments of radiative transfer (i.e., treatments more appropriate for stellar/planetary atmospheres than stellar/planetary interiors). How does accounting for the outermost, optically thin layers of planetary envelopes, naked before their host stars, affect how they grow? How does core accretion play out in the transparent cavities of transitional discs? Does the rcb enjoy the same immunity to the outer nebular density when the layers above it are optically thin? This paper seeks to answer these questions by grafting an Eddington two-stream atmosphere (Guillot 2010) onto our previous core accretion model (Lee et al. 2014; Piso & Youdin 2014). The model is detailed in section 2 and its output reviewed in section 3. Limitations to our opacity tables restrict these main results to stellocentric distances of  $\sim 0.1$  AU, where nebular temperatures are on the order of 1000 K. Nevertheless, in section 4.1, we experiment with alternative opacities and outline some semi-quantitative considerations that will enable us to explore how planets get their gas at larger distances, with particular attention paid to whether “super-puff” planets still need to acquire their gas beyond  $\sim 1$  AU (Lee & Chiang 2016). We place our work on atmospheric accretion into context with others’ work on atmospheric erosion in section 4.2, and wrap up in section 5.

## 2 MODEL

We study how a rocky core accretes a gas envelope from a disc that is optically thin to incoming starlight. Our procedure follows that of Lee et al. (2014) (see also Piso & Youdin 2014). We first construct one-dimensional hydrostatic snapshots of the planet, each having a unique gas-to-core mass ratio. Then we string the snapshots together along a timeline by calculating the time it takes to cool from one snapshot to the next. What is different in this paper is that we no longer assume the entire envelope to be optically thick; instead, we account for how the uppermost regions of the envelope can be optically thin to incoming visible and/or outgoing ther-

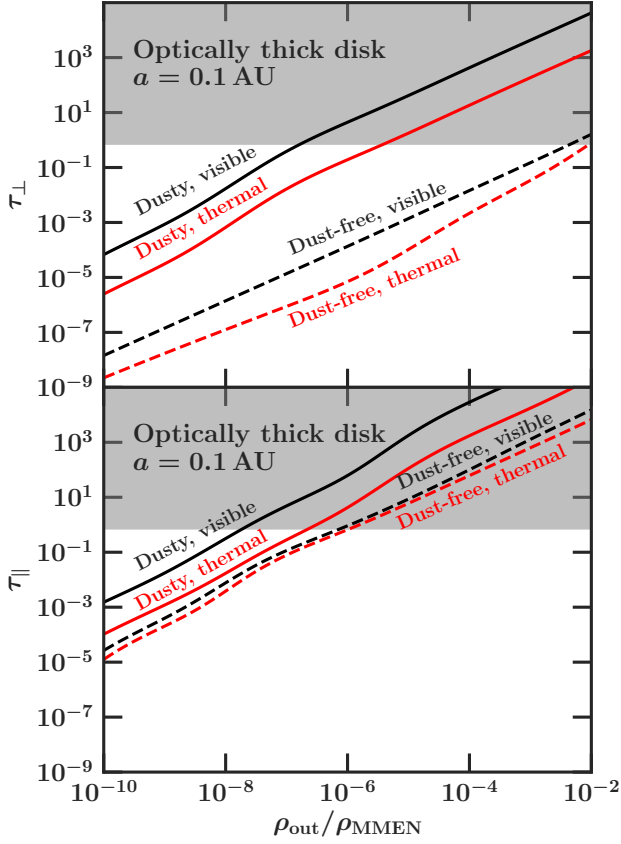


**Figure 1.** Parent disc densities that are low enough to be relevant for the formation of super-Earth atmospheres (Lee et al. 2014; Lee & Chiang 2016) may also be low enough to render the disc optically thin. Vertical optical depths  $\tau_{\perp}$  are computed for an isothermal disc at temperature 1000 K and an orbital radius of  $a = 0.1$  AU, starting from the midplane and integrating across three vertical scale heights. Midplane densities  $\rho_{\text{out}}$  are normalized to that of the minimum-mass extrasolar nebula,  $\rho_{\text{MMEN}} = 6 \times 10^{-6} \text{ g cm}^{-3} (a/0.1 \text{ AU})^{-2.9}$  (Chiang & Laughlin 2013). Radial optical depths  $\tau_{\parallel}$  are computed by integrating from  $a = 0.02$  AU to 0.1 AU. Opacities from Ferguson et al. (2005) are used, assuming metals either take the form of grains with an ISM-like size distribution (“dusty”) or are fully in the gas phase (“dust-free”). Optical depths at stellar wavelengths (“visible”) are evaluated as Planck means at a host star temperature  $T_{\star} = 5800$  K; at wavelengths characterizing disc-generated radiation (“thermal”), they are computed as Planck means at 1000 K. The results of this figure inform our choices for  $\rho_{\text{out}}$  in the rest of this paper; for dusty core accretion models, we study  $\rho_{\text{out}} \leq 10^{-5} \rho_{\text{MMEN}}$ , and for dust-free models,  $\rho_{\text{out}} \leq 10^{-3} \rho_{\text{MMEN}}$  (these choices are motivated by  $\tau_{\perp}$  rather than  $\tau_{\parallel}$  to explore a wider range of  $\rho_{\text{out}}$ , but  $\tau_{\parallel}$  is the more relevant for deciding whether planets are exposed directly to stellar irradiation).

mal radiation. The goal is to quantify how much the properties of the outer envelope affect the gas accretion rate.

## 2.1 Optically Thin Outer Layer

In the outermost portions of the gas envelope, where material is optically thin to either incident or internally generated

radiation, we solve the following stellar structure equations:

$$\frac{dM}{dr} = 4\pi r^2 \rho \quad (1)$$

$$\frac{dP}{dr} = -\frac{GM(<r)}{r^2} \rho \quad (2)$$

$$\frac{d\tau}{dr} = -\kappa_{\text{th}} \rho \quad (3)$$

$$\frac{4T^3 dT}{dr} = \left[ \frac{3}{4} T_{\text{int}}^4 - \frac{3\sqrt{3}\gamma}{4} T_{\text{eq}}^4 \left( \frac{\gamma}{\sqrt{3}} - \frac{1}{\gamma\sqrt{3}} \right) e^{-\gamma\sqrt{3}\tau} \right] \frac{d\tau}{dr} \quad (4)$$

where  $G$  is the gravitational constant,  $r$  is the radius from the center of the planet,  $\rho$ ,  $P$ , and  $T$  are the density, pressure, and temperature of the gas,  $M(<r)$  is the mass enclosed within  $r$ ,  $\kappa_{\text{th}}$  is the opacity to internal thermal emission (evaluated as a Planck mean; see equation 10 and surrounding discussion),  $\tau$  is the corresponding radial optical depth (with  $\tau = 0$  at the outermost radius  $R_{\text{out}}$ , defined as the Hill or Bondi radius, whichever is smaller, and increasing inward to the core). We will elaborate on  $\kappa_{\text{th}}(r)$ , and on the constants  $T_{\text{int}}$ ,  $T_{\text{eq}}$ , and  $\gamma$ , in what follows.

Equation (4) is derived from the temperature profile of an Eddington two-stream atmosphere (e.g., Guillot 2010):

$$T^4 = \frac{3T_{\text{int}}^4}{4} \left[ \frac{2}{3} + \tau \right] + \frac{3T_{\text{eq}}^4}{4} \left[ \frac{2}{3} + \frac{1}{\gamma\sqrt{3}} + \left( \frac{\gamma}{\sqrt{3}} - \frac{1}{\gamma\sqrt{3}} \right) e^{-\gamma\sqrt{3}\tau} \right]. \quad (5)$$

The atmosphere is heated from below by outgoing internal radiation (the first term) and from above by incoming stellar radiation (the second term). The internal radiation is generated by cooling of the entire envelope. The outgoing flux  $\sigma T_{\text{int}}^4$  is emitted at the thermal photosphere  $R_{\text{ph,th}}$  such that

$$T_{\text{int}}^4 \equiv \frac{L}{4\pi\sigma R_{\text{ph,th}}^2} \quad (6)$$

where  $\sigma$  is the Stefan-Boltzmann constant and  $L$  is the total internally generated luminosity from the envelope. The quantities  $R_{\text{ph,th}}$  and  $L$  are solved as part of our numerical procedure; they are not simple inputs. The incoming stellar flux is averaged over the entire planetary surface:

$$T_{\text{eq}}^4 \equiv \frac{T_{\star}^4}{4} \left( \frac{R_{\star}}{a} \right)^2 \quad (7)$$

where  $T_{\star}$  is the stellar effective temperature (= 5800 K for this paper),  $R_{\star}$  is the stellar radius (=  $1R_{\odot}$ ), and  $a$  is the planet’s orbital distance (= 0.1 AU). For these parameter choices,  $T_{\text{eq}} = 883$  K.

Whether the incoming stellar or the outgoing internal flux contributes more to the heating at a given location depends on the ratio of the “visible” and “thermal” opacities:

$$\gamma \equiv \frac{\kappa_{\text{vs}}}{\kappa_{\text{th}}} \quad (8)$$

where  $\kappa_{\text{vs}}$ , evaluated as a Planck mean (see equation 9 and

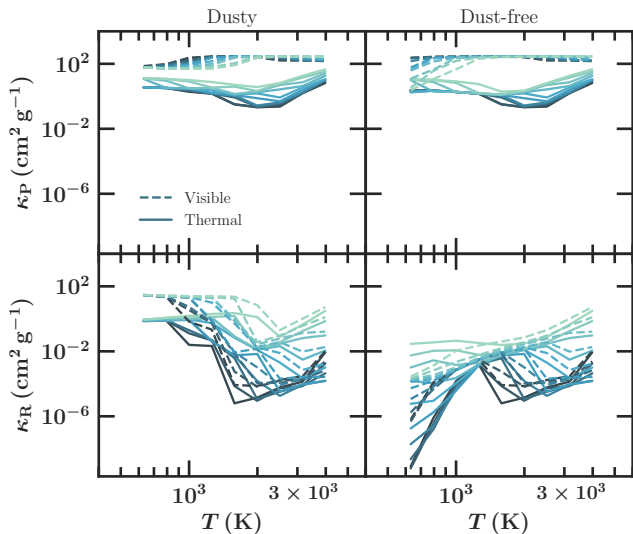


**Figure 2.** Opacities vs. temperature and density. Dark blue to light green colors correspond to  $\log \rho (\text{g cm}^{-3}) \in [-17, -15.5, -14, \dots, -3.5]$ . As  $T$  varies on the abscissa, the equilibrium chemical composition of the gas (+ dust in dusty models) changes according to the equilibrium calculations of [Ferguson et al. \(2005\)](#). Opacities are computed as either Planck ( $\kappa_P$ ) or Rosseland ( $\kappa_R$ ) averages; “visible” opacities evaluate the blackbody radiation field at the stellar temperature  $T_* = 5800$  K, while “thermal” opacities evaluate the blackbody function at the local  $T$ . Only Planck means (shown in the top two panels) are used for our two-stream, optically thin outer layer (sections 2.1 and 2.2); we revert to Rosseland means below the visible-light or thermal photosphere, whichever is deeper. Over most temperatures and densities, the visible  $\kappa_P$  is two orders of magnitude greater than the thermal  $\kappa_P$  (hence  $\gamma \equiv \kappa_{\text{vs}}/\kappa_{\text{th}} \sim 240$ , as indicated in Figure 5), with dust making little difference since the Planck mean is dominated by absorption lines of gaseous atoms and molecules (Figure 3).

surrounding discussion), is the opacity to the bulk of the radiation coming from the star (which is at visible wavelengths for our choice of  $T_* = 5800$  K, but can in principle be in any wavelength range). When the envelope has strong absorbers in the visible ( $\gamma \gg 1$ ), the stellar flux tends to dominate the heating ( $T^4 \sim T_{\text{eq}}^4 \gamma e^{-\gamma \sqrt{3} \tau}$ ; temperature decreases inward). In the opposite limit ( $\gamma \ll 1$ ), the internal flux tends to control the heating ( $T^4 \sim T_{\text{int}}^4 (2/3 + \tau)$ ; temperature increases inward).

Equation (5) assumes that  $\gamma$  is spatially constant; we choose to evaluate it at the outermost radius  $R_{\text{out}}$ . Although  $\gamma$  is held constant in a given snapshot,  $\kappa_{\text{th}}$  is calculated anew for every position  $r$ ; by extension,  $\kappa_{\text{vs}}$  also varies with depth. We now turn to how we compute  $\kappa_{\text{th}}$  and  $\kappa_{\text{vs}}$  (the latter only at  $R_{\text{out}}$ ).

## 2.2 Opacities

Wavelength ( $\lambda$ ) specific opacities  $\kappa(\lambda, \rho, T)$  are generated from a modified version of the stellar atmosphere code PHOENIX as described in [Ferguson et al. \(2005\)](#), assuming solar metallicity ( $Z = 0.02$ , where elemental abundances are

scaled to those in [Grevesse & Noels 1993](#)). Two different flavours of opacity models are explored: “dusty,” in which an ISM-like grain size distribution is assumed, and “dust-free,” in which metals never take the form of dust and are instead in the gas phase at their full abundances. The Ferguson et al. opacities incorporate heavy atomic metals such as iron, and in this regard appear more complete than other opacity tables (e.g., [Freedman et al. 2014](#)). At the low pressures and high temperatures characterizing our highly distended gas envelopes, atomic lines at short wavelengths ( $\lesssim 0.2 \mu\text{m}$ ) contribute significantly to  $\kappa_{\text{vs}}$ . We have found that excluding the heavy atoms decreases  $\kappa_{\text{vs}}$  by 1–2 orders of magnitude.<sup>3</sup>

The opacities  $\kappa_{\text{vs}}$  and  $\kappa_{\text{th}}$  are computed as Planck means:

$$\kappa_{\text{vs}}(\rho, T) \equiv \frac{\int \kappa(\lambda, \rho, T) B(\lambda, T_*) d\lambda}{\int B(\lambda, T_*) d\lambda} \quad (9)$$

$$\kappa_{\text{th}}(\rho, T) \equiv \frac{\int \kappa(\lambda, \rho, T) B(\lambda, T) d\lambda}{\int B(\lambda, T) d\lambda}, \quad (10)$$

the former using the Planck function  $B$  evaluated at the stellar temperature  $T_*$ , and the latter at the local gas temperature  $T$ . The use of Planck means is not entirely justified. In the derivation by [Guillot \(2010; see, e.g., his equation 16\)](#), the wavelength-averaged opacities are weighted by the mean intensity  $J$ . The problem is that  $J$  is not known *a priori*. We have chosen to replace  $J$  with the local Planck intensity  $B$ . An alternative is to replace equation (9) and/or (10) with the Rosseland mean (e.g., [Rogers et al. 2011](#)), but the Planck mean seems preferable since we are considering regions optically thin to both incoming starlight and outgoing internal radiation. [Hubeny et al. \(2003\)](#) also use Planck mean opacities for their atmospheres.

In principle, one need not adopt the same kind of mean for both  $\kappa_{\text{vs}}$  and  $\kappa_{\text{th}}$ . For example, if the envelope is optically thick to visible light but optically thin to its own thermal radiation, then it would seem appropriate to use the Rosseland mean for  $\kappa_{\text{vs}}$  and the Planck mean for  $\kappa_{\text{th}}$ . But this choice can lead to internal inconsistencies; as Figures 2 and 3 show, the Rosseland mean  $\kappa_{\text{vs}}$  can be significantly smaller than the Planck mean  $\kappa_{\text{th}}$ , which would not fit with our original supposition that the atmosphere be thick in the visible and thin in the infrared. We avoid this problem and simply adopt Planck means for both  $\kappa_{\text{vs}}$  and  $\kappa_{\text{th}}$ . Our choice of Planck means also accords better with our assumption of a spatially constant  $\gamma$ ; in Figure 2, we see that our Planck means change much less than our Rosseland means with temperature and density. Thus our Planck means afford our two-stream solution greater self-consistency.

The ambiguities in the choice of mean opacities underscore the limitations of using a constant- $\gamma$  atmosphere to describe what is really more complicated. Although the two-stream model used here cannot claim accuracy, it hopefully suffices to explore, in a qualitative way, the effect of the outermost atmospheric layers on the gas accretion rate.

<sup>3</sup> In an extensional calculation in §4.1, we will replace the [Ferguson et al. \(2005\)](#) opacities with the [Freedman et al. \(2014\)](#) opacities. Although the latter are missing the gas-phase heavy metals, they do extend to lower temperatures, enabling us to explore models at 1 AU instead of our standard 0.1 AU.

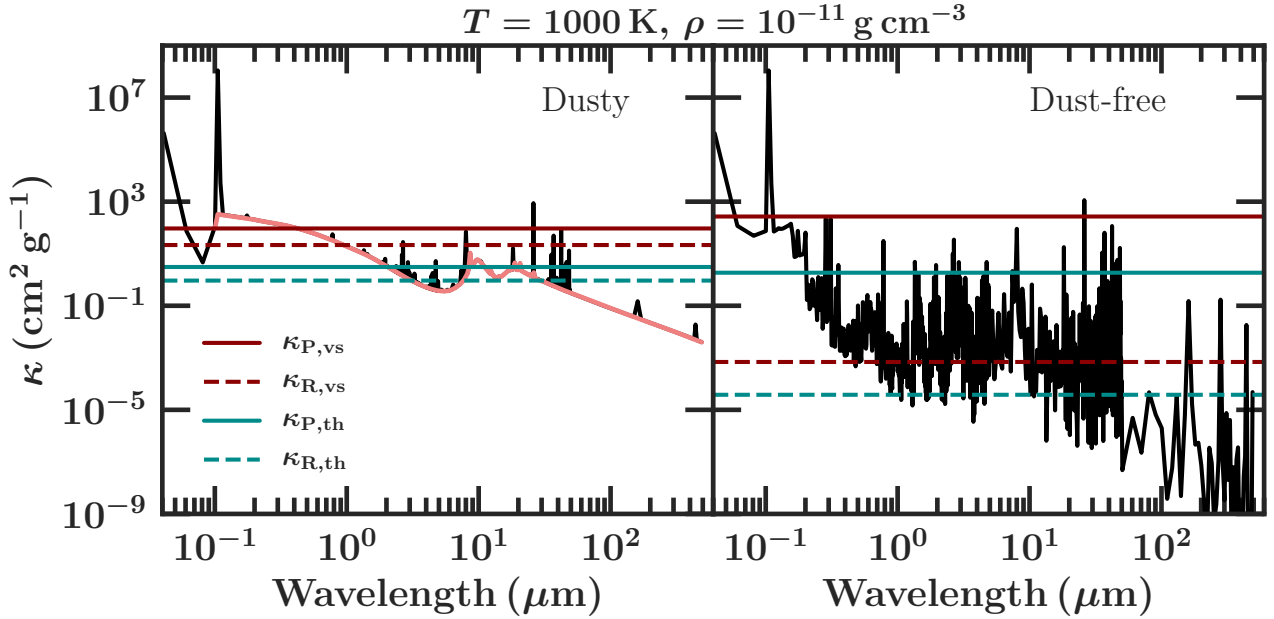


**Figure 3.** Opacity vs. wavelength (black curve) at fixed temperature  $T = 1000\text{ K}$  and density  $\rho = 10^{-11}\text{ g cm}^{-3}$ . Horizontal lines mark mean opacities, evaluated either as Planck (P) or Rosseland (R) averages, with the blackbody radiation field evaluated for either  $T_* = 5800\text{ K}$  (vs) or  $T$  (th). We employ Planck means for our optically thin, two-stream atmospheres, and Rosseland means for the interior below. Dust (left panel) contributes a strong continuum opacity (thick orange curve) that is absent from the dust-free model (right panel); consequently, the Rosseland means (dashed horizontal lines), which are more sensitive to the continuum than to absorption peaks, are much higher in dusty than dust-free models. By contrast, the Planck means (solid horizontal lines) do not vary much between dusty and dust-free models because they are more sensitive to absorption peaks, arising here from atomic Fe ( $\sim 0.1\ \mu\text{m}$ ) and oxides (TiO between  $0.4\ \mu\text{m}$  and  $1.2\ \mu\text{m}$ , CO near  $4\ \mu\text{m}$ , and water at longer wavelengths).

Comparison with full radiative transfer models would be welcome.

Figure 2 shows  $\kappa_{\text{vs}}$  and  $\kappa_{\text{th}}$  for a range of densities and temperatures. Dusty and dust-free models feature similar Planck mean opacities (compare top left and top right panels). In particular, the dusty model betrays no drop in opacity at  $T \gtrsim 1500\text{ K}$ , despite dust grains sublimating at those temperatures. Planck means (unlike Rosseland means) are sensitive to opacity peaks, and not to the continuum opacity controlled by dust. The strongest peaks are from gas absorption lines: from atomic iron at  $\sim 0.1\ \mu\text{m}$  and molecular species (e.g., CO, H<sub>2</sub>O, and oxides like TiO) at 1–40  $\mu\text{m}$  wavelength. The iron lines are also responsible for rendering  $\kappa_{\text{vs}}$  1–2 orders of magnitude higher than  $\kappa_{\text{th}}$ . In the literature, TiO and VO (which our opacity tables include) are often quoted as the strongest absorbers in the visible (e.g., Hubeny et al. 2003), but this claim is based on models that include only alkali metals, and not iron, in their repository of atoms. Atmospheres like ours that absorb strongly in the visible and weakly in the infrared (i.e., atmospheres with  $\gamma \gg 1$ ) exhibit temperature inversions, as we will see in section 3.

### 2.3 Overall Procedure

Our procedure is the same as that in Lee et al. (2014), except that in addition to iterating on  $L$ , we also iterate on  $T_{\text{int}}$  in the construction of each snapshot. Only a particular pair of

values  $L$  and  $T_{\text{int}}$  can satisfy equations (1)–(4) for a given set of outer boundary conditions, a given core mass  $M_{\text{core}}$ , and a given gas-to-core mass ratio  $\text{GCR} \equiv M_{\text{gas}}/M_{\text{core}}$ . For all models in this paper, we fix  $M_{\text{core}} = 5 M_{\oplus}$ ,  $R_{\text{core}} = 1.6 R_{\oplus}$ ,  $a = 0.1\text{ AU}$ ,  $T_{\text{eq}} = 883\text{ K}$ , and a nebular temperature  $T_{\text{out}} = 1000\text{ K}$ . The outer nebular density  $\rho_{\text{out}}$  is scanned over a range of values whose maximum is that of a fiducial gas-rich disc,  $\rho_{\text{MMEN}} = 6 \times 10^{-6}\text{ g cm}^{-3}$ . For these parameter choices, following section 2.1.1 of Lee et al. (2014),  $R_{\text{out}}$  equals the Hill radius of the planet ( $\sim 40 R_{\oplus}$ ).

For the above parameters, and for a given GCR, we proceed as follows:

- (i) Take the density of the envelope “surface” at  $r = R_{\text{out}}$  to equal the nebular density  $\rho_{\text{out}}$ .
- (ii) Guess  $L$ .
- (iii) Calculate a provisional value for  $R_{\text{ph,th}}$  as that radius where the (thermal, Planck mean) optical depth  $\tau = 2/3$ , assuming an isothermal outer atmosphere at temperature  $T = T_{\text{eq}}$  and integrating inward from  $R_{\text{out}}$ . Using this  $R_{\text{ph,th}}$  and  $L$ , calculate a provisional value for  $T_{\text{int}}$  using (6).
- (iv) Obtain the envelope surface temperature (not to be confused with the nebular temperature  $T_{\text{out}}$ ) by inserting  $\tau = 0$  into (5).
- (v) Evaluate  $\gamma$  using the envelope density and temperature at  $\tau = 0$  (and Planck mean opacities).
- (vi) Integrate equations (1)–(4) from  $R_{\text{out}}$  down to either the thermal photosphere  $R_{\text{ph,th}}$  or the visible-light photo-

sphere  $R_{\text{ph,vs}}$ , whichever is deeper (for our model parameters,  $R_{\text{ph,th}}$  is deeper). Use Planck mean opacities throughout.

(vii) From the resultant  $R_{\text{ph,th}}$ , re-calculate  $T_{\text{int}}$  using (6). If this  $T_{\text{int}}$  matches the provisional value of step (iii) (within 1%), then proceed to the next step; otherwise, return to step (iv) using this  $T_{\text{int}}$ .

(viii) Continue to integrate the stellar structure equations down to the radius of the solid core, swapping out equations (3) and (4) for the usual equations of radiative diffusion and convective energy transport (equations 5–8 of Lee et al. 2014, with opacities now evaluated as Rosseland means).

(ix) If the resultant envelope gas mass matches the desired value to within some tolerance ( $\sim 10^{-5}$ – $10^{-6} M_{\oplus}$ ), then the hydrostatic snapshot is complete; otherwise, return to step (ii).

Snapshots are constructed in order of increasing GCR and placed on a timeline that extends up to  $t_{\text{disc}} = 1$  Myr, the assumed disc lifetime (more precisely, the time over which  $\rho_{\text{out}}$  is held constant, after which the nebular density is assumed to fall to zero).

### 3 RESULTS

Figure 4 reveals that the rate of gas accretion does not much change when more careful account is made of the outer optically thin layer, as long as the outer nebular density  $\rho_{\text{out}}$  exceeds  $10^{-8} \rho_{\text{MMEN}}$ . For the same model parameters and at a given time, gas-to-core ratios in our new “optically thin” models typically differ by less than a factor of 2 from those of less realistic “radiative diffusion” models (i.e., models that utilize the equation of radiative diffusion even when the atmosphere is optically thin). Cores can only accrete as much gas as can cool (e.g., Lee & Chiang 2015), and the rate at which gas cools is governed by the radiative-convective boundary (rcb). That boundary, as demonstrated in Figure 5, sits well below the visible and thermal photospheres; the temperature and pressure at the rcb remain practically unchanged between most optically thin models and their radiative diffusion counterparts. This is true whether the opacities are for dusty or dust-free gas. Large temperature inversions appear in the uppermost layers, effected by strong absorbers at visible wavelengths (gas-phase atoms such as iron that render  $\gamma = \kappa_{\text{vs}}/\kappa_{\text{th}} \sim 240 \gg 1$ ; see section 2.2). But this upstairs drama does not seem to much affect the rcb downstairs.

What sets the temperature and density of the rcb, and what connection do they have, if any, to the outer optically thin layers? The situation is easiest to understand for dusty envelopes, whose rcb’s are located where  $\text{H}_2$  starts to dissociate (Lee et al. 2014). Dissociation of  $\text{H}_2$ , governed by Saha-type considerations, mandates the rcb temperature to be  $T_{\text{rcb}} \simeq 2500$  K. As for the rcb density  $\rho_{\text{rcb}}$ , that is determined by both the rcb temperature and the interior adiabat. In the convective zone below the rcb, the adiabatic index drops below  $4/3$  because energy is spent dissociating  $\text{H}_2$  instead of heating the gas, and the envelope mass becomes concentrated toward the rocky core (Lee & Chiang 2015). Thus  $\rho_{\text{rcb}}$  in dusty atmospheres is determined by the core radius, the envelope mass, the internal adiabat, and  $T_{\text{rcb}}$ , none of which is affected by the outer optically thin layers.

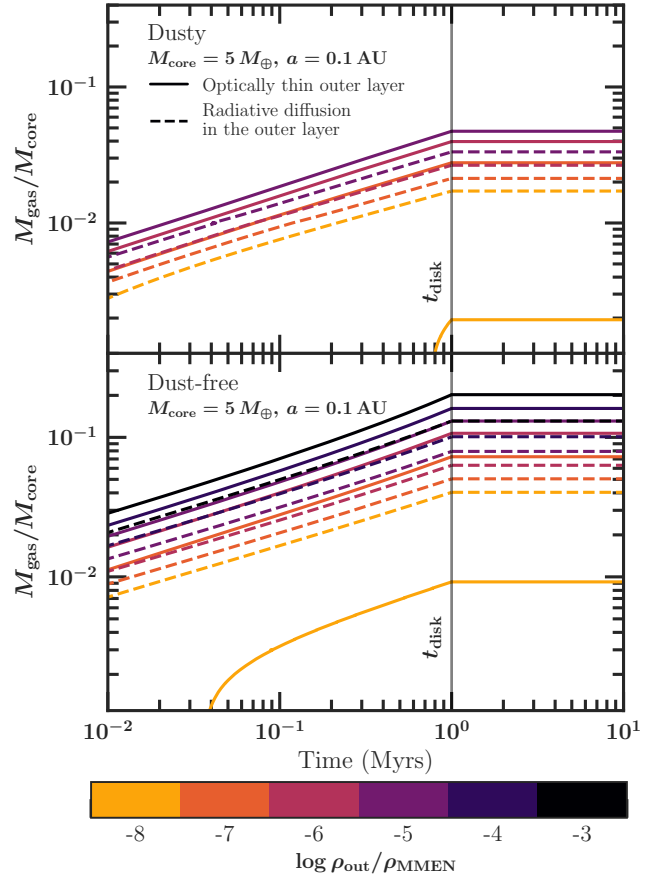


**Figure 4.** How close-in super-Earths ( $M_{\text{core}} = 5M_{\oplus}$  at  $a = 0.1$  AU) get their gas. As long as the nebular density  $\rho_{\text{out}}$  exceeds  $10^{-8} \rho_{\text{MMEN}}$  (see color bar), our new models that treat more carefully the planet’s outermost optically thin layers (solid curves) do not much differ from our previous models that rely only on the diffusion equation to describe radiative layers (dashed curves). Final gas-to-core mass ratios of  $\sim 1$ – $10\%$ , similar to those inferred from observations, result over many orders of magnitude variation in the background nebular density. Gas accretion is halted at an assumed disc lifetime of  $t_{\text{disc}} = 1$  Myr; it is clear from the displayed curves that shifting  $t_{\text{disc}}$  to 0.1 Myr (or even shorter times) would still succeed in generating percent-by-weight atmospheres. There are fewer curves in the dusty (top) panel because dust grains render atmospheres more opaque; dusty envelopes develop outer optically thin layers only for the more extreme nebular depletion factors (see Figure 1).

Dust-free envelopes are more complicated to diagnose. To a crude approximation we can describe them as isothermal (within a factor of  $\sim 2$ ) from the thermal photosphere down to the rcb (see bottom panels of Figure 5). In the radiative diffusion models, the temperature in this isothermal layer is set by the nebular temperature  $T_{\text{out}} = 1000$  K. For our new models with optically thin layers, this temperature is set instead by the thermal photosphere:  $T_{\text{ph,th}}^4 \sim T_{\text{int}}^4 + T_{\text{eq}}^4/2$ , as follows from inserting  $\tau = 2/3$  and  $\gamma \gg 1$  into equation (5). At 0.1 AU,  $T_{\text{eq}} \sim 883$  K while  $T_{\text{int}} \sim 100$ – $200$  K, and so  $T_{\text{ph,th}} \sim 0.84 T_{\text{eq}} \sim 740$  K. Since  $T_{\text{ph,th}}$  is close to  $T_{\text{out}}$ , it is not surprising that the new optically thin models behave similarly to the old radiative diffusion models.

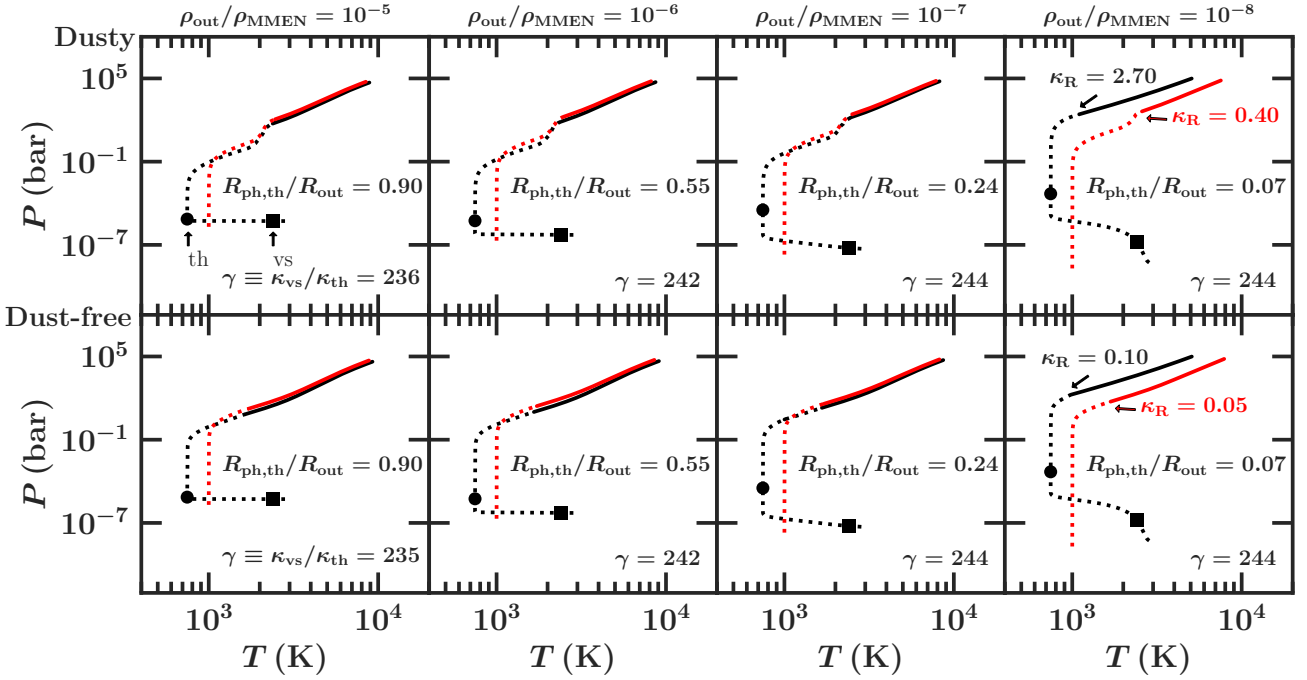


**Figure 5.** Atmospheric  $P$ - $T$  profiles of optically thin (black) and more primitive radiative diffusion (red) models at fixed  $GCR \equiv M_{\text{gas}}/M_{\text{core}} = 0.15M_{\oplus}/5M_{\oplus} = 0.03$ . The visible (vs) and thermal (th) photospheres (where  $\tau = 2/(3\sqrt{3}\gamma)$  and  $2/3$ , respectively) are marked by squares and circles, respectively. Because  $\gamma = \kappa_{\text{vs}}/\kappa_{\text{th}} \gg 1$ , the visible photosphere lies above the thermal, and there are strong temperature inversions captured only by the optically thin model. Regardless, the radiative-convective boundaries—where the radiative zones (dashed lines) connect with the convective zones (solid lines)—are practically identical between the optically thin and radiative diffusion models. Over a wide range of nebular depletion factors  $\rho_{\text{out}}/\rho_{\text{MMEN}} \geq 10^{-7}$ , pressures and temperatures of the rcb’s differ by at most factors of 2 between the two classes of model. Only when  $\rho_{\text{out}}/\rho_{\text{MMEN}} = 10^{-8}$  do the model rcb’s diverge strongly: the optically thin model features a higher density at its rcb, and thus a higher opacity (as annotated in cgs units) and a lower cooling/accretion rate. At these ultra-low nebular densities, differences between the two radiative transfer treatments become accentuated as the rcb is pushed close to the rocky core and the envelope becomes nearly completely radiative.

Technically, because of our temperature inversion,  $T_{\text{ph,th}}$  is slightly lower than  $T_{\text{out}}$ , which in turn lowers  $T_{\text{rcb}}$  in the optically thin models. The lower  $T_{\text{rcb}}$  and hence higher cooling luminosity explain why the gas accretion rates in optically thin models are systematically higher than in the radiative diffusion models; see how most of the solid curves in Figure 4 are higher than their dashed curve counterparts, not just in dust-free models but also in dusty ones. Just the opposite effect occurs when there is no temperature inversion, i.e., when  $\gamma \ll 1$ , as in Figure 7 discussed below. We will explore further how  $T_{\text{ph,th}}$  tracks  $T_{\text{out}}$ , and by extension how  $T_{\text{rcb}}$  is sensitive to the external nebular environment for dust-free atmospheres, in section 4.1.

The situation changes once the ambient disc is depleted in gas by more than eight orders of magnitude relative to our fiducial gas-rich minimum-mass extrasolar nebula. Under these extremely depleted conditions, our treatment of the outer optically thin layers impacts more significantly the growth and structure of the envelope as a whole. In Figure 4, we see that for  $\rho_{\text{out}}/\rho_{\text{MMEN}} = 10^{-8}$ , the final gas-to-core mass ratios of the optically thin models (dusty or dust-free) are approximately an order of magnitude smaller than those of the corresponding radiative diffusion models. The reason for this drop is that the rcb has been pushed

closer to the surface of the underlying rocky core, and with the envelope more nearly completely radiative, differences between how we treat the radiative transfer become magnified. Extremely gas-poor environments demand that atmospheric density profiles be sufficiently steep to contain a given amount of gas within the planet’s Hill sphere, and this steepening pushes the thermal photosphere deeper into the envelope (compare the black dotted curves in the right and second-from-right panels of Figure 5); the rcb is, of course, pushed inward as well. For  $\rho_{\text{out}}/\rho_{\text{MMEN}} = 10^{-8}$ , the thermal photospheres of the dusty and dust-free optically thin models are only about twice the radius of the rocky core, and the corresponding rcb densities and opacities are 2–10 times larger than those of the radiative diffusion models. These larger rcb densities and opacities lower the radiative luminosities, slowing cooling and by extension accretion—hence the especially low gas-to-core ratios seen in Figure 4 characterizing  $\rho_{\text{out}}/\rho_{\text{MMEN}} = 10^{-8}$ . At even lower nebular densities (data not shown), the rcb can be pushed all the way to the rocky core—i.e., the envelope becomes purely radiative—at which point the model sequence terminates (see also the isothermal endmember models in Lee & Chiang 2015, their Figure 4 and related discussion).

Although the models shown in Figure 4 are technically

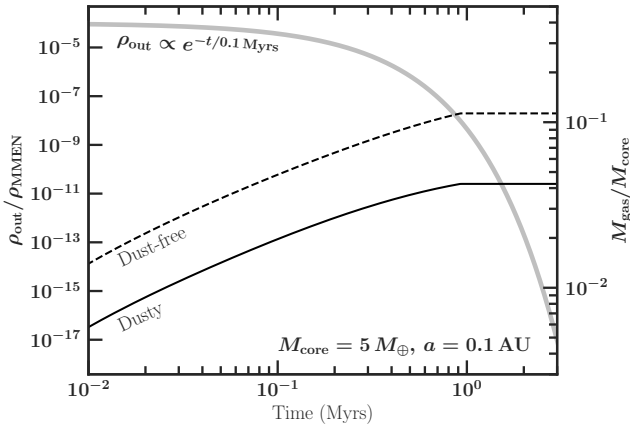


**Figure 6.** How  $5M_{\oplus}$  cores build their envelopes in an exponentially depleting nebula. The gas-to-core mass ratio (GCR  $\equiv M_{\text{gas}}/M_{\text{core}}$ ; solid and dashed curves using the right-hand axis) are computed by first fitting a scaling relationship to our numerical results for GCR vs. nebular density (we find GCR  $\propto \rho_{\text{out}}^{0.1}$ ), and then integrating over the time-derivative of GCR as the nebular gas depletes with an e-folding time of 0.1 Myr (gray curve using the left-hand axis). We halt envelope growth once  $\rho_{\text{out}}/\rho_{\text{MMEN}}$  falls below  $10^{-8}$  since the rate of gas accretion slows considerably (by about an order of magnitude compared to  $\rho_{\text{out}}/\rho_{\text{MMEN}} = 10^{-7}$ ; see Figure 4) at this level of depletion.

those of nebulae whose gas densities are fixed from  $t = 0$  to  $t = 1$  Myr and drop to zero thereafter, they are still reliable guides for nebulae whose gas densities deplete smoothly over time. The very fact that rates of gas accretion change only by factors of  $\sim 3$  when the nebular density varies by 4 orders of magnitude suggests that the detailed time history of nebular depletion introduces, at most, only order-unity effects. This expectation is confirmed in Figure 6 which shows how super-Earths amass  $\sim 4$ – $10\%$ -by-mass gas envelopes in a nebula that decays exponentially with an e-folding timescale of 0.1 Myr.

## 4 DISCUSSION

### 4.1 Creating Super-Puffs Beyond 1 AU

So far in this paper, we have concentrated exclusively on planets located 0.1 AU from their central stars. This restriction is due to our use of opacities generated from the model of [Ferguson et al. \(2005\)](#), which do not extend to the lower temperatures ( $\lesssim 500$  K) characterizing more distant regions of the disc. In this subsection we swap out the [Ferguson et al. \(2005\)](#) opacities for the opacities from [Freedman et al. \(2014\)](#) which do not have this limitation, in order to explore how atmospheric accretion unfolds at larger stellocentric distances. The drawback is that the [Freedman et al. \(2014\)](#) opacity model lacks the gas-phase heavy atomic metals (e.g., Fe) that may dominate the visible/ultraviolet wavelength opacity (see section 2.2).<sup>4</sup> We cannot expect the

<sup>4</sup> Whether such strong absorbers in the visible are actually present is unclear. Introducing them creates temperature inver-

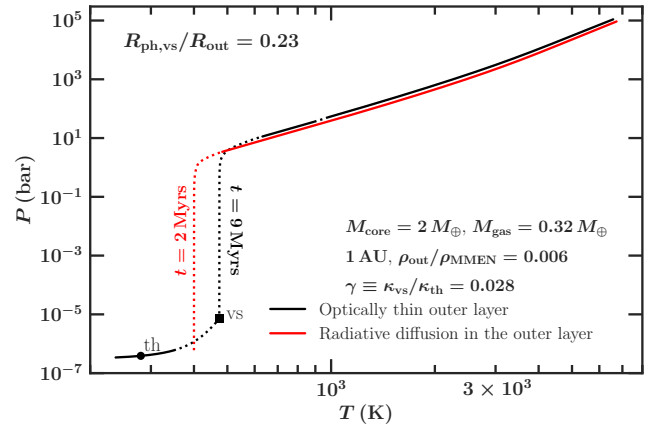


**Figure 7.** Atmospheric  $P$ - $T$  profile of a nascent super-puff ( $2M_{\oplus}$  core, GCR = 16%) in a depleted disc at 1 AU ( $\rho_{\text{out}} = 0.006 \rho_{\text{MMEN}} = 4 \times 10^{-11} \text{ g cm}^{-3}$ ). Figure notation is identical to Figure 5. The similarity of the radiative-convective boundaries between the optically thin and radiative diffusion models implies that the former’s more careful accounting of radiative transfer does not much matter; the narrative for super-puff formation told by [Lee & Chiang \(2016\)](#) should still hold. To create this figure, we resorted to the dust-free opacity table of [Freedman et al. \(2014\)](#) which extends to the cooler temperatures characterizing 1 AU at the cost of omitting heavy metals. For these opacities,  $\gamma \equiv \kappa_{\text{vs}}/\kappa_{\text{th}} = 0.028 \ll 1$  and so there is no stratospheric temperature inversion (cf. Figure 5). Gas accretes at a somewhat slower rate in the optically thin model than in the radiative diffusion model (note, as annotated, the difference in times at which the profiles are taken) because the rcb of the former materializes at a deeper layer where densities and temperatures are higher, resulting in a lower cooling luminosity  $L$ . These differences are probably overestimated by our model, which formally selects the innermost rcb to evaluate  $L$ ; that innermost rcb is located, in the optically thin model, at the base of a tiny radiative window that opens up within the convective zone at  $T \simeq 900$  K. We regard this feature as a possible artifact of our implementation of the [Piso & Youdin \(2014\)](#) method, in which it is not obvious which rcb to choose in evaluating  $L$  when there are multiple rcb’s. To obtain a more accurate  $L$  (and one that may vary with position in the envelope) would require the use of a more sophisticated code such as [MESA \(Paxton et al. 2011\)](#).

resultant calculation to be accurate, but hope to identify rough, qualitative trends.

The specific question we want to address is whether, with our more careful accounting of the outer optically thin layers, the formation channel of “super-puffs” identified by [Lee & Chiang \(2016\)](#) remains viable. Super-puffs are especially large ( $R \gtrsim 4 R_{\oplus}$ ) and low mass ( $M \lesssim 6 M_{\oplus}$ ) plan-

sions (see, e.g., our Figure 5) that might be present in some extrasolar planets (e.g., the hot Jupiters WASP-33b and WASP-121b; [Haynes et al. 2015](#); [Evans et al. 2016](#)) but have not been observed in others (e.g., HD 209458b; [Diamond-Lowe et al. 2014](#); [Line et al. 2016](#)). Heavy-metal atoms can gravitationally settle/rain out of atmospheres. We have verified that our main result—that the cooling rates of optically thin models and radiative diffusion models differ by factors less than 2—is robust against the inclusion/exclusion of heavy metals.



ets having gas-to-core ratios of  $\sim 20\text{--}40\%$ . In Lee & Chiang (2016; see also Inamdar & Schlichting 2015), the envelopes of super-puffs are dust-free and accrete at distances  $\gtrsim 1$  AU. The requirement that the envelopes be dust-free better couples the rcb temperature to the outer nebular temperature (the buffering effects of dust are absent); that nebular temperature, in turn, is lower at larger stellocentric distances. Molecular ro-vibrational modes freeze out in colder gas so the opacity drops; more transparent envelopes cool faster and therefore grow faster, enabling the production of super-puffs. How does this picture change with a more realistic treatment of the envelope's outermost, optically thin layers?

The answer is not by much, as judged by Figure 7: both our new optically thin model and the radiative diffusion model are on their way to forming a super-puff planet ( $M_{\text{core}} = 2M_{\oplus}$ , GCR = 16%). The models yield similar interior structures and have similar gas accretion histories.

A key feature of our super-puff theory is the sensitivity of the rcb to the external temperature (for dust-free atmospheres). This sensitivity persists in our new optically thin treatment. To within factors of 2, the rcb temperature is that of the deepest photosphere. For  $\gamma \gg 1$ , the deepest photosphere is the one evaluated at thermal (infrared) wavelengths:

$$T_{\text{ph,th}}^4 \sim T_{\text{int}}^4 + T_{\text{eq}}^4/2. \quad (11)$$

For  $\gamma \ll 1$ , the deepest photosphere is the visible-light photosphere:

$$T_{\text{ph,vs}}^4 \sim T_{\text{int}}^4/\gamma + T_{\text{eq}}^4/\gamma \quad (12)$$

obtained by substituting  $\tau \sim 1/\gamma$  into equation (5); recall that  $\tau$  by definition is the optical depth at thermal, not optical wavelengths. In either case, as long as the external irradiation temperature  $T_{\text{eq}}$  exceeds the internal temperature  $T_{\text{int}}$ , the rcb will respect the former and cool down at larger stellocentric distances.

Far from the star, the inequality will reverse: the irradiation temperature  $T_{\text{eq}}$  will fall below the internal temperature  $T_{\text{int}}$ , and the rcb may lose its sensitivity to the external environment. We estimate at what stellocentric distance this happens by assuming that  $T_{\text{eq}} > T_{\text{int}}$  and seeing where this assumption breaks down. The assumption implies that

$$T_{\text{rcb}} \sim T_{\text{ph,th}} \sim T_{\text{eq}}/2^{1/4} \quad (13)$$

for  $\gamma \gg 1$ , and

$$T_{\text{rcb}} \sim T_{\text{ph,vs}} \sim T_{\text{eq}}/\gamma^{1/4} \quad (14)$$

for  $\gamma \ll 1$ . To convert these into relations between  $T_{\text{eq}}$  and  $T_{\text{int}}$ , we replace  $T_{\text{rcb}}$  with  $T_{\text{int}}$  using (6), in combination with equations (13) and (23) of Lee & Chiang (2015) for the luminosity:

$$L \sim 4 \times 10^{23} \text{ erg s}^{-1} \left( \frac{480 \text{ K}}{T_{\text{rcb}}} \right)^{4.5} \left( \frac{0.3}{\text{GCR}} \right)^{1.6} \left( \frac{M_{\text{core}}}{2M_{\oplus}} \right)^{4.6} \quad (15)$$

where we have taken the adiabatic index  $\gamma_{\text{ad}} = 1.3$ . Substituting (15) into (6) and taking  $R_{\text{ph}} = 0.9R_{\text{out}}$  (where  $R_{\text{out}}$  is the Bondi radius for  $M_{\text{core}} = 2M_{\oplus}$  and a gas temperature of  $T_{\text{out}} = 1000(a/0.1 \text{ AU})^{-3/7}$  K; for  $a = 1\text{--}100$  AU, it is smaller than the Hill radius), we solve for  $T_{\text{int}}$  in terms of  $T_{\text{rcb}}$ , and from there obtain relations between  $T_{\text{int}}$  and  $T_{\text{eq}}$

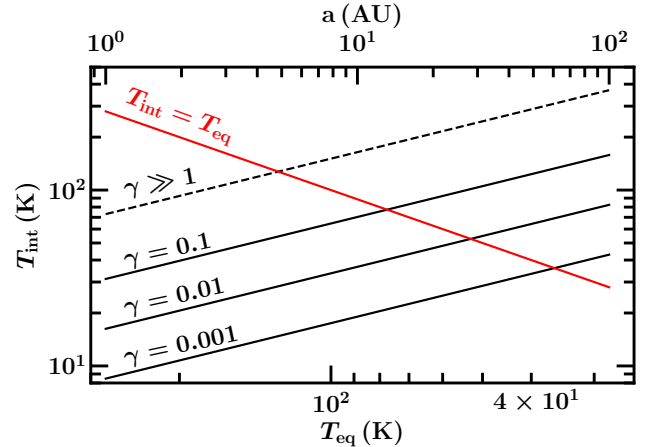


**Figure 8.** Estimating where in the disc we can expect the external irradiation temperature  $T_{\text{eq}}$  to dominate the internal temperature  $T_{\text{int}}$  in controlling the rcb temperature  $T_{\text{rcb}}$  of nascent super-puffs ( $M_{\text{core}} = 2M_{\oplus}$ , GCR = 0.3). The black lines trace  $T_{\text{int}}$  vs.  $T_{\text{eq}}$  for various values of  $\gamma$  and are computed as follows: we first evaluate the cooling luminosity  $L$  in equation (15), taking  $T_{\text{rcb}} = T_{\text{eq}}/2^{1/4}$  for  $\gamma \gg 1$  and  $T_{\text{rcb}} = T_{\text{eq}}/\gamma^{1/4}$  for  $\gamma < 1$ ; we then substitute this  $L$ , and  $R_{\text{ph}} = 0.9R_{\text{out}}$  (where  $R_{\text{out}}$  equals the Bondi radius, which is smaller than the Hill radius for the parameters of this plot), into equation (6) to solve for  $T_{\text{int}}$ . This procedure assumes  $T_{\text{eq}} > T_{\text{int}}$  (so that  $T_{\text{eq}}$  controls  $T_{\text{rcb}}$ ) and so the resultant black curves are only self-consistent up until they intersect the red  $T_{\text{int}} = T_{\text{eq}}$  line. We see that the assumption  $T_{\text{eq}} > T_{\text{int}}$  is valid within  $\sim 5$  AU for  $\gamma \gg 1$  and out to larger distances for smaller  $\gamma$ . These are the distances out to which we can expect the rcb temperatures of dust-free planetary atmospheres to respect the external irradiation temperature, or in other words, the distances out to which we can expect the growth and evolution of atmospheres, including those of super-puffs, to be sensitive to the incident stellar flux.

from (13) and (14). The resultant relationships between  $T_{\text{int}}$  and  $T_{\text{eq}}$  are shown in Figure 8 as black lines. The underlying assumption  $T_{\text{eq}} > T_{\text{int}}$  is seen to be self-consistent out to  $\sim 5$  AU if  $\gamma \gg 1$  and out to larger distances for smaller  $\gamma$ . Inside these distances, the growth of super-Earth/super-puff atmospheres respects the external nebular temperature  $T_{\text{eq}}$  (and not the nebular density); outside these distances, we expect atmospheric growth to enter an asymptotic regime that is insensitive to both nebular temperature and nebular density.

## 4.2 Atmospheric Mass Loss

Our concern has been with how atmospheres grow during the gas disc depletion phase. But atmospheres can also lose mass in disc-depleted environments (Ikoma & Hori 2012; Owen & Wu 2013, 2016, 2017; Ginzburg et al. 2016, 2017). As we explain below, atmospheric erosion generally takes place after, and does not interfere with, the atmospheric accretion phase that we have been exploring in this paper and earlier ones in our series.

In the process of cooling-limited accretion that we have been studying, the cooling time of the atmosphere  $t_{\text{cool}}$

(equivalently, the gas accretion timescale) adjusts to the disc depletion timescale  $t_{\text{disc}}$ . A necessary condition for the atmosphere to erode instead of accrete is  $t_{\text{cool}} > t_{\text{disc}}$  (Ikoma & Hori 2012; Owen & Wu 2016).

Two ways have been discussed in the literature to achieve this inequality. In one way,  $t_{\text{disc}}$  suddenly becomes shorter than  $t_{\text{cool}}$ . In the “two-timescale” view of disc dispersal, the nebula transitions from depleting on a slow timescale to a fast one (Clarke et al. 2001; Alexander et al. 2014). As soon as this switch occurs, the nebular pressure that once confined the planetary envelope suddenly lifts, allowing over-pressured atmospheric gas to escape across the Hill/Bondi boundary, either as a breeze or as a wind (Ikoma & Hori 2012; Owen & Wu 2016). This way of triggering atmospheric mass loss is not relevant for our scenario of late-time super-Earth formation, which posits that rocky cores form after disc gas has largely (but not completely) gone away. That is, our story for super-Earth formation takes place wholly during the fast and final second stage of nebular dispersal, after the switch has already occurred (an explicit demonstration of atmospheric growth taking place entirely during the fast nebular dispersal phase is given by Figure 6, which shows growth even when  $t_{\text{disc}}$  is as short as 0.1 Myr—the cooling timescale  $t_{\text{cool}}$  simply adjusts to match  $t_{\text{disc}}$ ).

The second way to achieve  $t_{\text{cool}} > t_{\text{disc}}$  is by lengthening  $t_{\text{cool}}$ . Long cooling times characterize the latest atmospheric accretion stages, when the nebula is most heavily depleted and the radiative-convective boundary (rcb) of the envelope approaches the underlying rocky core (see our discussion toward the end of section 3 of the case  $\rho_{\text{out}}/\rho_{\text{MMEN}} \leq 10^{-8}$ ). When the inner convective zone shrinks to a thickness comparable to the radius of the core, it becomes possible for the envelope’s thermal energy to fall below the core’s thermal energy—this is the case when GCR  $\lesssim 5\%$  (Ginzburg et al. 2016; Ginzburg et al. 2017). Under these conditions, it becomes energetically possible for heat from the core to blow off the entire atmosphere (Ikoma & Hori 2012). Whether it actually does so depends on a number of factors. First, the planet must be close enough to its host star that, even though the rcb has retreated to near the core, the outer radiative envelope remains hot and distended out to the Hill/Bondi radius, i.e., the wind’s sonic point (embodied in equation 7 of Ginzburg et al. 2017; see also Fulton et al. 2017 for possibly related observations). Second, for the core to drive atmospheric mass loss effectively, it must transport its energy efficiently, by internal convection; a model assumption has been that the core is isothermal at the same temperature as the gas right above it—that the core and envelope cool in lockstep at a rate controlled by the radiative-convective boundary of the envelope (Ikoma & Hori 2012; Ginzburg et al. 2017). Whether core convection might be too sluggish and fail to carry away enough heat is an unresolved issue (see the large mantle viscosities considered by Stamenković et al. 2012 which imply core cooling timescales as long as 0.1–10 Gyr). A third factor is the efficiency with which core heat is converted into a mechanical wind; this efficiency has been assumed to be unity (Ginzburg et al. 2017) but radiative losses from the envelope will lower it.

If core power is not significant at driving mass loss, then an outflow can still derive from the heat of the atmosphere itself (Ikoma & Hori 2012; Owen & Wu 2016; Ginzburg et al. 2016; Ginzburg et al. 2017). Such winds are expected to be

modest. Owen & Wu (2016) find that planetary gas mass fractions can be reduced by factors of 10 or more, but these are overestimates insofar as most of the mass of their convective atmospheres was assumed to be located at large radii. More realistically, the adiabatic index  $\gamma_{\text{ad}} < 4/3$  in the convective interior, which renders the atmospheric mass concentrated toward the core (see section 1). For reference, in most of our accretionary models,  $\lesssim 20\%$  of the envelope mass is in outer radiative zones.

Finally, the heating required to drive outflows may be provided externally, by stellar photoionizing radiation at ultraviolet and X-ray wavelengths which can heat atmospheric gas to temperatures exceeding several thousand K. Photoevaporative winds can shave away or even destroy entirely the atmospheres of the closest-in super-Earths, at orbital periods shorter than about 10 days (Owen & Wu 2013, 2017; Fulton et al. 2017). Photoevaporative erosion takes place on  $\sim 100$  Myr timescales, when stellar coronal activity remains significant, and long after the entirety of the gas disc has been purged (and replaced with a stellar wind).

## 5 SUMMARY

Our study has shown that the theory of core accretion can work just as well in optically thin environments as it does in optically thick ones. Although core accretion has traditionally been treated in wholly optically thick envelopes, assumed to be embedded in optically thick circumstellar discs (e.g., Pollack et al. 1996), our calculations have demonstrated that how planetary atmospheres grow does not much change when the ambient disc density is reduced to values so low that the disc and large portions of the envelope are transparent. In particular, super-Earths can accrete their  $\sim 1\%$ -by-mass atmospheres, and super-puffs their  $\sim 20\%$ -by-mass atmospheres, in discs depleted by many orders of magnitude—up to seven in our model—relative to a conventional gas-rich minimum-mass nebula. Such discs can have vertical optical depths to visible-wavelength starlight as low as  $10^{-5}$  and radial optical depths as low as  $10^{-1}$  at stellocentric distances of 0.1 AU.

Lee & Chiang (2016) have advocated the optically thin cavities of “transitional” discs as natural birth sites for super-Earths and their atmospheres. Their calculations of core accretion were not always strictly self-consistent, as they utilized the equation of radiative diffusion to describe energy transport even when photons in the thermal infrared were able to free stream through gas envelopes. Our work addressed this shortcoming by computing more realistically how radiation is transferred in the outermost, optically thin layers of planetary atmospheres. We found that such an accounting can have dramatic impact on the envelope’s outermost temperature structure, potentially producing, e.g., strong stratospheric temperature inversions due to heavy metals (e.g., atomic Fe). But such high-altitude complications are more-or-less immaterial for the cooling and hence gas accretion history of the planet. Numerous studies (e.g., Piso & Youdin 2014; Lee & Chiang 2015; Lee & Chiang 2016; Ginzburg et al. 2016) have cited the primacy of the envelope’s radiative-convective boundary (rcb) in controlling that history. Our work reinforces this point. We have taken care in the present work to distinguish the visible and

thermal photospheres of the envelope, but the rcb, lying at much greater depths, behaves much as it does in earlier radiative diffusion models. In particular, if gas is laden with dust, it remains true that the rcb properties are determined by H<sub>2</sub> dissociation and not by any of the details of the upper atmosphere; and if gas is free of dust, it is also still true that the rcb temperature tends to follow the temperature of the upper atmosphere, which is set by stellar irradiation for planets within a few AU of their host stars. Our work supports the picture of Lee & Chiang (2016) that planets get their gas in parent discs that are themselves nearly empty of gas; the rates of planetary gas accretion that they computed are lower than ours by factors on the order of 2. Only when there is so little nebular gas that the rcb is pushed all the way to the surface of the underlying rocky core (see also Ginzburg et al. 2017) does our gas accretion rate drop significantly compared to the previous work.

We have emphasized, here and in Lee & Chiang (2016), how in dust-free atmospheres, the rcb temperature tracks the temperature of the outer layers, specifically the temperature of the visible or infrared photosphere, whichever is deeper. This connection implies that more gas-rich planets—gas giants and super-puffs—form more easily at large stellocentric distances where atmospheres are colder and therefore optically thinner, cooling and growing more rapidly. However, this connection between the nebular environment and the rcb eventually breaks down. Far enough away from the host star, the incident radiation on the planet will be too feeble to heat significantly the atmospheric layers above the rcb. For these distant planets, the rcb temperature will asymptote to a value that does not depend on stellocentric distance but will be set instead by the primordial heat of formation (whatever energy was brought in by accreting gas). The factors controlling the ability of the disc to spawn gas-rich planets will no longer include stellar irradiation, but will involve the availability of solid materials and the efficiency with which those solids can be assembled into cores. These are issues that we are currently investigating.

## ACKNOWLEDGMENTS

We are grateful to Richard Freedman and Mark Marley for in-depth conversations that helped us understand opacities better. We also thank Jeff Cuzzi, Kevin Heng, Jack Lissauer, Nikku Madhusudhan, Eliot Quataert, and Leslie Rogers for helpful and motivating discussions. Andrew Youdin provided positive and constructive feedback on our submitted manuscript, and Michiel Lambrechts delivered a thoughtful and encouraging referee’s report that led to substantive improvements. EJL was supported in part by NSERC of Canada under PGS D3, the Berkeley Fellowship, and the Sherman Fairchild Fellowship at Caltech. EC acknowledges support from the NSF. This research used the Savio computational cluster resource provided by the Berkeley Research Computing program at the University of California, Berkeley, supported by the UC Berkeley Chancellor, Vice Chancellor for Research, and Chief Information Officer.

## REFERENCES

Alexander R., Pascucci I., Andrews S., Armitage P., Cieza L.,

- 2014, in Beuther, H. and Klessen, R. S. and Dullemond, C. P. and Henning, T. ed., , *Protoplanets and Protostars VI*. The University of Arizona Press
- Batalha N. M., et al., 2013, *ApJS*, **204**, 24
- Burke C. J., et al., 2015, *ApJ*, **809**, 8
- Chiang E., Laughlin G., 2013, *MNRAS*, **431**, 3444
- Clarke C. J., Gendrin A., Sotomayor M., 2001, *MNRAS*, **328**, 485
- Diamond-Lowe H., Stevenson K. B., Bean J. L., Line M. R., Fortney J. J., 2014, *ApJ*, **796**, 66
- Dong S., Zhu Z., 2013, *ApJ*, **778**, 53
- Espaillet C., et al., 2014, *Protostars and Planets VI*, pp 497–520
- Evans T. M., et al., 2016, *ApJ*, **822**, L4
- Ferguson J. W., Alexander D. R., Allard F., Barman T., Bodnarik J. G., Hauschildt P. H., Heffner-Wong A., Tamanai A., 2005, *ApJ*, **623**, 585
- Freedman R. S., Lustig-Yaeger J., Fortney J. J., Lupu R. E., Marley M. S., Lodders K., 2014, *ApJS*, **214**, 25
- Fressin F., et al., 2013, *ApJ*, **766**, 81
- Fulton B. J., et al., 2017, *AJ*, **154**, 109
- Ginzburg S., Schlichting H. E., Sari R., 2016, *ApJ*, **825**, 29
- Ginzburg S., Schlichting H. E., Sari R., 2017, preprint, ([arXiv:1708.01621](https://arxiv.org/abs/1708.01621))
- Grevesse N., Noels A., 1993, *Origin and Evolution of the Elements*. Cambridge University Press
- Guillot T., 2010, *A&A*, **520**, A27
- Haynes K., Mandell A. M., Madhusudhan N., Deming D., Knutson H., 2015, *ApJ*, **806**, 146
- Howard A. W., et al., 2010, *Science*, **330**, 653
- Hubeny I., Burrows A., Sudarsky D., 2003, *ApJ*, **594**, 1011
- Ikoma M., Hori Y., 2012, *ApJ*, **753**, 66
- Inamdar N. K., Schlichting H. E., 2015, *MNRAS*, **448**, 1751
- Lee E. J., Chiang E., 2015, *ApJ*, **811**, 41
- Lee E. J., Chiang E., 2016, *ApJ*, **817**, 90
- Lee E. J., Chiang E., Ormel C. W., 2014, *ApJ*, **797**, 95
- Line M. R., et al., 2016, *AJ*, **152**, 203
- Lopez E. D., Fortney J. J., 2014, *ApJ*, **792**, 1
- Owen J. E., Wu Y., 2013, *ApJ*, **775**, 105
- Owen J. E., Wu Y., 2016, *ApJ*, **817**, 107
- Owen J. E., Wu Y., 2017, preprint, ([arXiv:1705.10810](https://arxiv.org/abs/1705.10810))
- Owen J. E., Ercolano B., Clarke C. J., 2011, *MNRAS*, **412**, 13
- Paxton B., Bildsten L., Dotter A., Herwig F., Lesaffre P., Timmes F., 2011, *ApJS*, **192**, 3
- Petigura E. A., Marcy G. W., Howard A. W., 2013, *ApJ*, **770**, 69
- Piso A.-M. A., Youdin A. N., 2014, *ApJ*, **786**, 21
- Pollack J. B., Hubickyj O., Bodenheimer P., Lissauer J. J., Podolak M., Greenzweig Y., 1996, *Icarus*, **124**, 62
- Rogers L. A., Bodenheimer P., Lissauer J. J., Seager S., 2011, *ApJ*, **738**, 59
- Rowe J. F., et al., 2014, *ApJ*, **784**, 45
- Stamenković V., Noack L., Breuer D., Spohn T., 2012, *ApJ*, **748**, 41
- Weiss L. M., Marcy G. W., 2014, *ApJ*, **783**, L6
- Wolfgang A., Lopez E., 2015, *ApJ*, **806**, 183
- Wu Y., Lithwick Y., 2013, *ApJ*, **772**, 74